Global tropospheric ozone responses to reduced NOx emissions linked to the COVID-19 world-wide lockdowns

Kazuyuki Miyazaki[1], Kevin Bowman[1], Takashi Sekiya[2], Masayuki Takigawa[2], Jessica L Neu[1], Kengo Sudo[3], Greg Osterman[1], and Henk Eskes[4]

[1]California Institute of Technology
[2]JAMSTEC
[3]Nagoya University
[4]Royal Netherlands Meteorological Institute

November 24, 2022

Abstract

Efforts to slow the transmission of COVID-19 led to rapid, global ancillary reductions in air pollutant emissions. Here, we quantify the resulting decreases in global NOx emissions and their consequent impact on the production of global tropospheric ozone using a multi-constituent data assimilation system. Total anthropogenic NOx emissions were reduced by at least 15% globally and 18-25% for Europe, North America, and the Middle East in April and May 2020. The efficacy of these reductions in altering ozone concentrations varied substantially in both space and time, with differences driven by local meteorology and chemical production efficiency. Globally, the total tropospheric ozone burden dropped by about 6 TgO 3 (2%) in May-June 2020, largely due to emission reductions in Asia and the Americas. Our results show a clear and global atmospheric imprint from COVID-19 mitigation, which altered the atmospheric oxidative capacity, climate radiative forcing, and human health.

Global tropospheric ozone responses to reduced NOx emissions linked to the COVID-19 world-wide lockdowns

Kazuyuki Miyazaki,[1*] Kevin Bowman,[1] Takashi Sekiya,[2]
Masayuki Takigawa,[2] Jessica L. Neu,[1] Kengo Sudo,[3] Greg Osterman,[1] Henk Eskes,[4]
[1]Jet Propulsion Laboratory, California Institute of Technology, Pasadena, CA, USA
[2]Japan Agency for Marine-Earth Science and Technology, Yokohama, 236-0001, Japan
[3]Graduate School of Environmental Studies, Nagoya University, Nagoya, Japan
[4]Royal Netherlands Meteorological Institute, De Bilt, the Netherlands

[*]E-mail: kazuyuki.miyazaki@jpl.nasa.gov.

Efforts to slow the transmission of COVID-19 led to rapid, global ancillary reductions in air pollutant emissions. Here, we quantify the resulting decreases in global NOx emissions and their consequent impact on the production of global tropospheric ozone using a multi-constituent data assimilation system. Total anthropogenic NOx emissions were reduced by at least 15% globally and 18-25 % for Europe, North America, and the Middle East in April and May 2020. The efficacy of these reductions in altering ozone concentrations varied substantially in both space and time, with differences driven by local meteorology and chemical production efficiency. Globally, the total tropospheric ozone burden dropped by about 6 TgO_3 ($\sim$2 %) in May-June 2020, largely due to emission reductions in Asia and the Americas. Our results show a clear

and global atmospheric imprint from COVID-19 mitigation, which altered the atmospheric oxidative capacity, climate radiative forcing, and human health.

Introduction

In order to slow the transmission of COVID-19, numerous countries worldwide have imposed lockdown measures that severely limit personal mobility, leading to reductions in overall economic activity (*1*). These measures were first enacted in Wuhan, China on January 23th, 2020, followed by Italy and then much of the rest of the world in March 2020. These restrictions on human activity were designed to alleviate the strain on the health care system from COVID-19 (*2*), but also had the ancillary impact of rapid air pollutant emission reductions. Changes in greenhouse gas (GHGs) and pollutant emissions have been estimated using activity data such as mobility metrics (*3–5*), with global NOx emissions estimated to have declined as much as 30% in April (*4*). However, these estimates are highly uncertain, as activity data is incomplete and significant assumptions are needed to relate these data to the partitioning and magnitude of emissions.

Substantial impacts on regional and global air quality during the COVID-19 period have also been demonstrated using various in-situ and satellite measurements (*6–10*). A study using the spatially-limited set of global surface in-situ air quality measurement networks estimated declines in population-weighted concentration of 60% for surface nitrogen dioxide (NO_2) and 31% for particulate matter smaller than 2.5 μm (PM2.5), and marginally significant increases of 4% in ozone between the beginning of the lockdowns and 15 May (*11*). These estimates highlight the different responses of surface concentrations for different species and the strong regional dependence of the response, but due to the sparseness of the in situ network they do not provide a truly global picture of the pandemic's impact on atmospheric composition.

Satellite measurements such as those from the TROPOspheric Monitoring Instrument (TROPOMI)

have captured the rapid reductions in tropospheric NO_2 columns, as well as in other species, associated with global COVID-19 lockdown measures (*7, 12*). However, the inference of emissions from the observed concentrations must account for variations in atmospheric transport, chemical environment, and meteorology (*13, 14*). Furthermore, because PM2.5 and ozone are the primary causes of premature mortality and other health effects of air pollution (*15*), their response to reduced NOx emissions is of particular interest. Tropospheric ozone is produced from its precursors, primarily NO_x and Volatile Organic Compounds (VOCs), through nonlinear chemical processes. It is not only important to human health, but also plays a crucial role in tropospheric chemistry and chemistry-climate interactions as the third most important anthropogenic greenhouse gas in the atmosphere (*16, 17*). Due to the dependency of ozone production on photochemical environment, its response to emission reductions is expected to vary substantially based on timing and location. However, the current in-situ observing network is too sparse to capture this variable response. Furthermore, the tendency toward sampling highly populated areas could lead to biased estimations when extrapolating from regional to global scales due to local titration effects. Although satellite measurements provide much denser sampling than surface networks, the lack of consistent long-term records of ozone from satellites (*18*).

In the decade prior to the COVID-19 pandemic, many countries implemented environmental policies to reduce human health risks associated with poor air quality. These policies largely focused on regulating air pollutant emissions through changes in human activity and through increased efficiency (i.e., technology). However, the actual air pollutant response to these policies cannot be directly measured because factors other than changes in emissions, such as meteorology and the background chemical state, affect air pollutant levels and can exhibit long-term variations that confound detection of emissions-driven changes (*13, 19*). COVID-19 represents a "scenario-of-opportunity" that informs our understanding of how air pollution levels respond to rapid and large reductions in human activity and concomitant air pollutant emissions. Anal-

ysis of the air pollution response to COVID-19 lockdown measures thus provides important information on effective environmental policy-making aimed at improving air quality. In addition, because tropospheric ozone and aerosols affect radiative forcing when lofted into the free troposphere, their response to changing emissions also sheds light on air quality-climate co-benefits (*16*).

This study quantifies the response of global tropospheric ozone to the unprecedented NOx emission reductions associated with COVID-19. This analysis is made possible by a new multi-constituent satellite data assimilation system (*20*) that ingests multiple satellite observations to simultaneously optimize concentrations and emissions of various trace gas species, while taking their complex chemical interactions into account. This framework was already used to quantify the surface air quality response to Chinese COVID-19 lockdown measures (*21*).

Results

Global NOx emission reductions Anthropogenic NOx emission reductions linked to the COVID-19 pandemic were estimated as the difference between baseline "business as usual" (BAU) emissions, obtained by aggregating 2010-2019 emissions from our decadal chemical reanalysis constrained by multiple satellite measurements (*20*), and 2020 emissions derived from the same system, using 2020 TROPOMI NO_2 observations. The BAU emissions were adjusted to 2020 values using the difference between the 2010-2019 baseline and 2020 emissions on February 1, when economic activity was not yet substantially affected by COVID-19 mitigation for most countries. For China, however, where the first government-imposed lockdown occurred earlier than in the rest of the world, the difference in emissions on January 10 is used to obtain the BAU emissions. Therefore, the 2020 COVID-19 emission anomaly, estimated as difference between the BAU and COVID-19 emissions, does not include the influence of climatological seasonal changes in anthropogenic emissions (see Materials and Methods for further

information). Biomass burning and soil NOx emissions, as well as areas that were heavily affected by clouds and at high latitudes (higher than 55°) were removed from the data assimilation analysis. The a priori emissions used in the data assimilation system have limited representation of actual ship tracks, which hinders evaluation of ship emission changes; NOx emissions over oceans were thus removed as well. Although our analysis covers about 75% of the global total NOx emissions, actual emission changes at country or global scales are likely larger than our estimates because of the unrepresented areas. Uncertainties on the COVID-19 emission anomalies were estimated from the interannual variability in the BAU emissions (see Materials and Methods for further information).

The NO_2 in the model simulation using the optimized emissions exhibits consistent variations with observed NO_2 columns (Figure S1). Meanwhile, the regional or country mean tropospheric NO_2 columns show strikingly different seasonal and spatial changes than the NOx emissions due to varying influences of non-linear chemical and meteorological conditions. For example, tropospheric NO_2 concentrations naturally decrease from winter through summer as a result of photochemical processes, even without any reduction in emissions.

Global total anthropogenic NOx emissions in 2020 were reduced by 9.0±1.5% relative to the global total emissions (12.8±2.1 % relative to the analyzed areas total emissions) in February, 12.7±1.5% (17.8±2.1 %) in March, 14.8±2.3% (21.2±3.3 %) in April, 15.0±1.8% (21.8±2.6 %) in May, and 13.9±1.8% (20.8±2.6 %) in June relative to the BAU emissions (Table 1 and Figs. 1 and 2). In February, the reduction in emissions from China made the largest contribution (36 %) to the global NOx anomaly, whereas the contributions from other regions defined in Fig. S2 are larger from March to June, when China relaxed its restrictions. Regional total emissions dropped by 18–25 % in April-May across Europe, North America, and the Middle East. Africa and South America also show clear but moderate reductions in emissions (∼ 5-10%) in April-May, with substantial spatial variations within the regions. The peak reduction

in global total NOx emissions of about 5 TgN per year is almost the same as the climatological annual anthropogenic emissions from Europe in our estimates. In many regions, the early emission reductions in February and March suggest that activity likely started decreasing even before actual implementation of lockdown measures, as further discussed below.

At the country scale, the estimated temporal evolution of emission reductions is strongly correlated with the COVID-19 Government Response Stringency Index (*22*), an indicator of the severity of government lockdown measures to slow transmission of COVID-19 (Fig. 3). The overall agreement between the NOx emission reductions and the Stringency Index suggests that our emission analysis is able to capture the rapid changes in emissions linked to government actions globally (Fig. S3). Chinese NOx emissions rapidly declined from late January through late February, corresponding to China's first lockdown, followed by a rapid recovery to their normal levels for March and April. In May, the emissions again started to decrease, with a maximum reduction of 8 % corresponding to a second lockdown in some parts of the country, such as Beijing, that was imposed to stop the second wave of COVID-19 cases. In Italy, the early implementation of lockdown led to large emission reductions, from late February to early May, of up to 25 %. For other European countries such as France and Spain, both large emission reductions and high values of the Stringency Index are found from March through May. The majority of states in the United States announced emergency stay-at-home orders in late March. The estimated emissions show declines beginning in late February and early March, prior to the implementation of restrictive measures, with maximum reductions of about 25 % in April and May, followed by a moderate recovery in June. These changes are broadly consistent with statistical data such as Google mobility data (*23*) and the Stringency Index (Fig. 3) and suggest that there was reduced traffic even before the stay-at-home-order. However, there were cloudy conditions in February and March over some US cities such as Los Angeles, which could have produced unstable emission corrections; this possibility will be explored further in

a follow-up study. In Mexico, a nationwide lockdown was imposed in late March, and the NOx emissions show a quick drop, with a maximum reduction of about 14 % in April. Several Middle Eastern counties, such as Saudi Arabia and Iran, also show emissions reductions of up to 25% from March through June, with a slight recovery in June. Limitations on human activity also affected emissions in South America. For instance, emissions from Brazil and Argentina were reduced by up to 10 and 15 %, respectively, from March through June. The larger reductions in Argentina correspond to the stronger government response than in Brazil. A large emission reduction was also found over Lima, Peru (up to 30 %) in April-May.

One of the confounding factors in attributing concentration changes to COVID-19 related emissions in tropical regions in Asia and central Africa is biomass burning, which is often related to agricultural regions near more populated areas. In order to migrate these impacts, we utilize MODIS burned area data as well as outliner filtering (for model grids with rapid emission increases) to exclude biomass burning emissions. Nevertheless, downwind regions may also be affected by enhanced NO_2 concentrations linked to fires. In addition, possible errors in the model transport could lead to artificial adjustments to anthropogenic emissions in top-down estimates. The anthropogenic emissions around fire areas could be better estimated by combining our top-down emissions estimates with in-situ surface measurements and bottom-up inventories. Such an analysis, however, is left to future work.

The estimated emission changes we show here are broadly consistent with those based on bottom-up emission estimates for the COVID-19 period (*3–5*). Nevertheless, the NOx emission estimates based on activity data (*4*) reveal larger global total emission reductions (about 30 % in April) than our estimates (14.8$\pm$2.3 % relative to the globe total emissions and 21$\pm$3.3 % for the analyzed area), with larger contributions from China (about 2.5 % of the global total emissions reduction, in contrast to 1.0 % in our estimate) and smaller contributions from Europe (about 2%, in contrast to 4%). Although the temporal changes in NOx are generally consistent

for major polluted countries, the bottom-up estimates indicate larger reductions in NOx, for instance, up to 40 % for the US (in contrast to 24 % relative to the global total emissions and 34% relative to the analyzed area total emissions for our top-down estimates), 57 % for Italy (25% and 32%), 64 % for Spain (32% and 34%), 54 % for Saudi Arabia (20% and 34%), 49 % for Mexico (14% and 32%), 52 % for Argentina (17% and 45%), and 43 % for Brazil (17% and 32%). These discrepancies could reflect large uncertainties in the activity data, which is limited to selected sectors, used in bottom-up estimates. In contrast, our top-down approach infers total emission changes, although the influence of model errors needs to be considered. Detailed comparisons of spatial and temporal emission patterns between the top-down and bottom-up estimates will play an essential role in the further exploration of the COVID emission anomaly.

Tropospheric ozone response Using the BAU emissions and 2020 emissions with the same meteorological conditions allows us to evaluate tropospheric ozone concentration changes directly linked to COVID-19 emissions declines while accounting for the ”observed” meteorology (as filtered through a reanalysis system, see Materials and Methods). This approach is in contrast to studies that evaluate atmospheric composition anomalies in 2020 directly from comparisons between 2020 conditions and previous years (*7, 11*). In such studies, the confounding factors of meteorological variations and spatiotemporal differences in the relationship between atmospheric concentrations and emissions adds substantial, but poorly constrained, uncertainty in their inferences of COVID-19 effects on atmospheric composition.

Our sensitivity simulations show a strong response of ozone to the COVID-19 NOx reductions that extends from the surface to the upper troposphere (Fig. 4). The results using our 2020 emissions show better agreement with observed concentrations from in-situ measurements, ozonesondes, and ozone retrievals from the Cross-Track Infrared Sounder (CrIS) satellite instrument (*24*) than those using BAU emissions for the globe (Fig. S4-S6 and Table

S1). At the local scale, and especially near the surface, the estimated ozone response varies greatly with location and time as a consequence of differences in photochemical regime, which depends on a number of factors other than NOx. These factors include the amount and reactivity of VOCs (climatological VOC emissions were used in all simulations, see Materials and Methods), background oxidant levels, and meteorological conditions. Over highly polluted urban areas with high NOx concentrations, additional NOx can suppress ozone production due to NOx titration; this response is mainly due to enhanced atmospheric oxidation capacity (AOC) in these locations, which is reflected in the levels of major oxidants (e.g. the hydroxyl radical (OH) and nitrate radical (NO_3)) (*25*). Therefore, NOx emission reductions can increase ozone locally over urban areas due to high levels of OH and reactions with VOCs. Increased surface ozone was seen in our estimates over parts of northern Europe, China, and south Africa, as has already been reported for northern China during the lockdown (*10, 21*). Nevertheless, the obtained ozone production efficiency (OPE, mass of ozone produced per unit mass of NOx emitted) for the monthly mean tropospheric ozone burden (TOB, in TgO_3 unit, integrated from the surface to the tropopause globally) based on the regional emission changes was mostly positive throughout the analysis period (i.e., NOx emission declines reduced TOB), as seen in other modelling studies (*26*).

While the globally-averaged tropospheric lifetime of ozone is relatively short (23 days) (*27*), it can be significantly longer in the free troposphere. Therefore, the influence of NOx emissions reductions on TOB can be accumulated during the course of the COVID pandemic. Thus, we evaluated cumulative total tropospheric ozone changes from model simulations starting in February 2020. As summarized in Fig. 5, the estimated ozone response shows substantial seasonal variations as a consequence of varying meteorological and chemical conditions in addition to emissions changes. In total, the global TOB decreased by 0.6 TgO_3 in February and by 6.5 TgO_3 in June, reflecting an order of magnitude intensification in the decline in just

over 5 months. The reduced ozone associated with the COVID-19 emissions accounted for about 2 % of TOB ($\sim$300 TgO_3) in May and June. Because areas that account for about 25 % of the global total anthropogenic NOx emissions were removed from our estimates, including tropical biomass areas with strong OPE, the actual ozone changes may be even larger. Assuming that the removed areas had similar relative emission reductions as the surrounding areas, we obtain a reduction of up to 9 TgO_3, about 3 % of TOB. By comparison, the most aggressive representative concentration pathway (RCP) defined for the Climate Model Intercomparison Project-5 (RCP 2.6) projects a reduction of TOB of about 4% by 2030 (*27*). Applying the average satellite-derived TOB trend over the past two decades (+0.71 TgO_3/yr, from -2.15 to + 2.85 TgO_3/yr for different satellite sensors) (*28*), the COVID-19 TOB reductions of 6-9 TgO_3 are equivalent to going back in time to TOB values for 2007-2011.

In order to identify regional and seasonal changes in the ozone response, we conducted sensitivity calculations in which we compared the BAU and 2020 emissions for each region separately. The contributions of emissions from each region to TOB varied substantially with time. In February, the large emission reductions in China had little impact on ozone. In March, Asia (including China) and South America account for about 60 % of the total ozone reduction (2.5 TgO_3). In April, the total reduction of 4.7 TgO_3 is mainly attributed to emission reductions in Asia, China, North America, and South America (0.7-0.8 TgO_3 for each region). In May and June, when the reduction in TOB reached its maximum value, the Asian emissions (excluding China, whose emissions had largely recovered by that time) have the largest contribution to the total ozone reduction (1.2-1.5 TgO_3 out of 6.0-6.5 TgO_3), followed by North America (1.2 TgO_3) and South America (0.8 TgO_3). The NOx emissions from the Middle East, Europe, Africa, and Australia provided minor contributions to the global ozone budget from February though June.

The ozone reductions corresponding to the emission decreases in each region exhibit distinct

spatial patterns, including both local and remote impacts (Fig. 4 and S7). For instance, free tropospheric ozone over Eastern and Central Eurasia is reduced due to North American emission reductions, whereas the South American emission reductions result in a long tail of decreased ozone along the mid-latitude westerlies in the SH. In all, the COVID-19 NOx reductions led to up to 10 ppb reductions in monthly mean ozone at the surface and 3 ppb reductions at 500 hPa (Figs. 4a and 4b). In terms of vertical propagation, the European and Australian emission influences on ozone are mostly limited to the region below 300 hPa and poleward of 30°. These patterns are likely dominated by quasi-isentropic transport linked to mid-latitude synoptic-scale disturbances. The ozone anomalies from the Middle Eastern, South American, and North American emissions extend up to 200 hPa in the subtropics through deep convection, with up to 1 ppb reductions in the monthly and zonal mean concentration in the upper troposphere (Figs. 4c and S8). Asian emissions show a distinct pattern, with maximum values of the ozone anomaly in the upper troposphere and the anomaly extending throughout the tropics to the mid latitudes of both hemispheres. This pattern reflects not only convection over the maritime continent, but also transport through the Asian monsoon, suggesting substantial impacts of Asian human activity on the global environment. The latitudinal and vertical propagation of ozone anomalies seen in Figs 4, S7, and S8, with 2-5 % reductions in the zonal mean concentration in the tropics and Northern Hemisphere (NH) subtropics and 1-2 % reductions in the Southern Hemisphere (SH) and NH extratropics, signifies important implications for ozone radiative forcing, as ozone has the largest impact on the top-of-atmosphere flux in the middle and upper troposphere (*29*). The NOx reductions could also affect radiative forcing through decreases in nitrate aerosol; the impacts on secondary aerosol formation need to be further addressed in a future study.

Reduced NOx emissions during the COVID period also led to decreases in free tropospheric peroxyacetyl nitrate (PAN) concentrations over both polluted regions (by up to about 35 ppt) and remote areas such as northern and southern Atlantic and Pacific oceans (by up to about 10

ppt; Fig. S9a). PAN is a long-lived reservoir species for NOx and can be transported long distances from source regions before decomposing; these results highlight the non-local impacts of the emission reductions on global ozone through long-range transport of precursors. Meanwhile, substantial reductions in tropospheric mean OH of up to 30 % locally (Fig. S9b) suggest substantial impacts of the worldwide lockdowns on the entire tropospheric chemistry system, including on the chemical lifetimes of many species such as methane. The maximum reduction of the tropospheric global mean OH concentration, which occurs in May, is 4.0 %.

The OPE was estimated using the TOB response corresponding to reduced NOx emissions for each month separately. The OPE increased by a factor of 2-5 from February to July in the NH mid and high latitudes (Table 2 and Fig. 5), largely due to the increasing availability of sunlight from the winter to the summer season. When averaged over the February to June time period, tropical and SH low and mid latitudes regions, such as Africa, South America, and Australia show much larger OPE values (1.9-2.9 TgO_3/TgN) than those in the NH extratropics (0.2-0.4 TgO_3/TgN). The OPE variations help to explain the different ozone response patterns described above. The impact of the large extratropical NH NOx emission reductions on tropospheric ozone is relatively small due to the weak OPE, especially in the winter and spring seasons. In contrast, ozone reductions are much larger for tropical regions such as South America, despite smaller NOx changes, because of the larger OPE. These results suggest that considering where and when government actions to slow the spread of COVID-19 occurred is extremely important in understanding the impacts of COVID lockdowns on atmospheric composition.

The response of ozone to changes in NOx emissions can differ significantly between chemical transport models. In our previous work using a multi-model chemical data assimilation system (*30*), we obtained up to a factor of 2 difference in surface ozone response among different models due to fundamental differences in the representation of fast chemical and dynamical processes. At the same time, multi-model inter-comparison studies have demonstrated that the

ozone response to varying NOx emissions in the MIROC-CHASER model (*31*) used here fits well within the multi-model estimates (*32–34*).

Our modeled ozone responses to COVID-19 NOx emissions are broadly consistent with observed ozone changes. Recently developed tropospheric ozone profile retrievals from the CrIS satellite instrument (*24*) provide an opportunity to evaluate the simulated ozone responses. The modeled ozone in the free troposphere shows closer agreement with the CrIS observations for many regions when using the 2020 emissions than when using BAU emissions (Fig. 6a). The discrepancy between CrIS and the BAU emissions scenario increases from April through June. The RMSE reduction associated with the COVID emissions reaches 20% in May and June, while the mean bias against the CrIS data in June is reduced by using the COVID emissions from 3.2 to 2.0 ppb in the SH and from 2.0 to 1.1 ppb in the NH. Furthermore, the RMSE between the model and surface measurements is reduced by 20-40 % for Europe, the United States, and China when considering the COVID-19 emission reductions (Figs. 6b, S5-S6, Table S1). Additional model evaluation results are provided in the Supplementary Materials (S1-S4).

In this paper, we have shown for the first time the impacts of COVID-related NOx emissions reductions on global tropospheric ozone, but there are additional considerations that should be investigated further to fully understand the implications of COVID-19 emission changes for ozone. For example, inconsistencies in TROPOMI sampling, mainly due to clouds, may have affected the estimated short-term variations in NOx emissions. Furthermore, although the model used has a relatively high spatial resolution for the globe (0.56 °), the simulation of surface concentrations is sensitive to model resolution, owing to the fine-scale distribution of emissions and transport as well as resolution-dependent non-linear effects in the NO_2 loss rate (*35*). Aerosol levels were also greatly affected by COVID-19 (*36*), which may have had an additional impact on ozone chemistry. Simultaneous reductions in primary aerosol and NOx emissions could have the effect of increasing ozone (*19*). The absence of changes in primary aerosol in our COVID

emissions estimates might explain some of the remaining model ozone bias, especially at the surface. In addition, while the NOx reductions were large enough that ozone sensitivity regimes in highly polluted areas may have shifted from VOC-limited to NOx-limited during the COVID lockdowns, the contribution of changes in VOCs needs to be addressed in future work, along with a means to validate the results.

Discussion

The worldwide actions taken to slow the transmission of COVID-19 had the effect of rapid emission reductions globally, which drove substantial changes in air pollutants and tropospheric chemistry. The pandemic took place against a backdrop in which many countries have implemented environmental policies to reduce human health risk from air pollution by controlling emissions, but the quantitative impacts of these policies have not always been clear (*37–39*). COVID-19 represents a well-observed "scenario-of-opportunity" that allows us to assess how air pollution levels respond to reduced human activity and emissions, providing an important benchmark for identifying effective environmental policy making. In this paper, we have evaluated global NOx emission reductions and their impacts on global tropospheric ozone, using a state-of-the-art multi-constituent data assimilation system.

The COVID-19 restrictions on human activity in numerous countries led to substantial reductions in global total anthropogenic NOx emissions of at least 15 % in April and May 2020, with 19-25% reductions in the US, Europe, and the Middle East. Using the estimated emission reductions, we find that the tropospheric ozone response to the NOx emission reductions exhibited strong spatial and temporal gradients as a consequence of differences in OPE, with larger values in the tropics and SH subtropics (1.9-2.9 TgO_3/TgN, February-June average) than in the NH mid- and high-latitudes (0.2-0.4 TgO_3/TgN). The OPE in the NH extratropics increased by a factor of 2-3 from February to June. The reduction in ozone associated with COVID-19

changes in NOx is as large as 10 ppb and is seen both at the surface and in free tropospheric concentrations. The COVID-related ozone anomaly is widespread in the NH and is substantial even in the SH, especially downwind of mega-cities in South America. Overall, the pandemic led to a 6 TgO_3 ($\sim$2%) decrease in TOB in May and June. Decreased concentrations of PAN and OH suggest highly non-local impacts of the lockdowns and substantial changes in the tropospheric chemistry system.

The results described here demonstrate the strong impacts of the worldwide restrictions on human activity on global tropospheric chemistry, human health, and radiative forcing, and will benefit future predictions of the chemistry-climate system by providing validation of our understanding of the response of tropospheric chemistry to changes in emissions. In addition, the designers of environmental policies to improve air quality need to consider the complex relationships between emissions and atmospheric composition demonstrated here carefully in order to effectively improve air quality and reduce its impacts on human health, especially for countries in the tropics that have a combination of high population density and large OPE. Finally, our ozone response estimates for the COVID-19 pandemic provide insights into where and when the atmospheric composition effects of the pandemic may be measurable directly from observations.

MATERIALS AND METHODS

Experimental Design The surface NOx emission reductions associated with the COVID-19 lockdowns were estimated using a top-down approach within a state-of-the data assimilation system (*20*). The obtained emission reductions were used to evaluate the tropospheric ozone response and OPE for each region of the world using the MIROC-CHASER global CTM.

Top-down surface NOx emission estimates An updated version of the Tropospheric Chemistry Reanalysis version 2 (TCR-2) (*20*) is used to evaluate NOx emission changes and their influence on ozone concentrations. The TCR-2 dataset is available at: `https://doi.org/10.25966/9qgv-fe81`. The reanalysis is produced via the assimilation of multiple satellite measurements of ozone, CO, NO_2, HNO_3, and SO_2. The tropospheric NO_2 column retrievals from the QA4ECV version 1.1 level 2 product for OMI (*40*) and TM5-MP-DOMINO version 1.2 for TROPOMI (*41*) were used to constrain NOx emissions. We employed a super-observation approach (*42*) to generate representative data with a horizontal resolution of the forecast model. The OMI SO_2 data used were the planetary boundary layer vertical column SO_2 L2 product obtained with the principal component analysis algorithm (*43*). The MOPITT total column CO data used were the version 7 L2 TIR/NIR product (*44*). Version 4.2 ozone and HNO_3 L2 products from MLS (*45*) were used to constrain the chemical concentrations in the upper troposphere and lower stratosphere. The model and data assimilation calculations for 2020 in this study were conducted at 0.56° horizontal resolution using the Model for Interdisciplinary Research on Climate (MIROC)-chemical atmospheric general circulation model for study of atmospheric environment and radiative forcing (CHASER) and an ensemble Kalman filter technique that optimizes both chemical concentrations of various species and emissions of NOx, CO, and SO_2.

The emissions estimation is based on a state augmentation technique, which has been employed in our previous studies (*30, 42, 46–49*). This approach allows us to reflect temporal and geographical variations in transport and chemical reactions in the emission estimates. The emissions in the state vector are represented by scaling factors for each surface grid cell. The quality of the reanalysis fields for 2005-2018 has been evaluated based on comparisons against ozonesondes as well as independent aircraft and satellite observations for various chemical species on regional and global scales, as well as for seasonal, yearly, and decadal scales, from

the surface to the lower stratosphere (*20*). The emissions for 2020 constrained by TROPOMI NO_2 at 0.56° horizontal resolution have already been used to evaluate the air quality response to the Chinese COVID-19 lockdown (*21*).

To evaluate emission anomalies due to the COVID-19 restrictions, the influence of climatological temporal emission variations was removed by comparing the 2020 optimized emissions with the baseline "business as usual" (BAU) emissions constructed based on our decadal chemical reanalysis, which is constrained by OMI NO_2 (*20*). The following steps were taken to obtain the BAU emissions for 2020 at each grid point. (1) The 2010-2019 emissions obtained from the reanalysis were used to evaluate relative temporal emission changes from February 1 (January 10 for China only) through July 31 each year. (2) The calculated relative temporal emission changes were averaged over the ten years (2010-2019) to obtain climatological relative emission variations. (3) The climatological relative emission variations were applied to the 2020 emission values on February 1, 2020 (January 10, 2020 for China) through July 31, 2020 to obtain the BAU emissions for 2020. Because the emissions changed only gradually during the non-COVID periods in the reanalysis, the choice of the base date did not affect the estimated COVID emission anomaly substantially. While the emission estimates based on long-term OMI records enabled us to evaluate climatological emission variations, assimilation of TROPOMI NO_2 for 2020 provided strong constraints on the detailed spatiotemporal variations in the 2020 COVID-19 emissions (Fig. S1). The influences of systematic biases between TROPOMI and OMI measurements, along with the influences of interannual changes in emissions, were excluded by aggregating the normalized temporal variability for each year.

Based on the comparisons between the 2020 and BAU emissions, we estimated the COVID emission anomaly, which eliminates the impacts of the climatological seasonal changes in emissions, such as the use of wintertime heating and enhanced soil emissions in summer, as well as interannual variations. In addition, in top-down estimates, systematic model errors, for instance

in the seasonally-varying chemical lifetime of NOx, can cause artificial seasonal changes in emissions, which are also removed by comparing the BAU and 2020 emissions constructed using the same system. Biomass burning signals in emissions were removed using MODIS burned area information (*50*), while surrounding grid points that were likely affected by fires (based on rapid emission increases) were also removed. Because of the relatively large uncertainty and limited coverage of the assimilated measurements, grid points poleward of 55° in both hemispheres and countries including those grid points (Canada, Russia, and northern Europe, except for the United Kingdom), as well as ocean grid points (i.e., ship emissions), were also excluded from the analysis. Areas that were heavily affected by clouds, as measured from variability of emission increments during the analysis period, were also removed from data assimilation analysis. In total, areas with about 25% of the global total NOx emissions were excluded from our analysis. For China, the impact of the Chinese New Year holiday was removed from the 2020 emissions to separately evaluate the COVID-19 anomaly using the baseline emission variations relative to the Chinese New Year date each year, following the method in our previous study (*21*).

Chemical transport model, MIROC-CHASER The forecast model used in the chemical data assimilation and sensitivity model calculations is MIROC-Chem (*31,51*) at 0.56° horizontal resolution. The model simulates spatial and temporal variations in chemical species in the troposphere and stratosphere by calculating tracer transport (advection, cumulus convection, and vertical diffusion), emissions, dry and wet deposition, and chemical processes (92 species, 262 reactions) including the ozone-HOx-NOx-CH_4-CO system with non-methane volatile organic compound oxidation. It also includes stratospheric chemistry such as halogen chemistry. The meteorological fields were calculated using the MIROC-AGCM atmospheric general circulation model (*31*). The simulated meteorological fields were nudged to the 6-hourly ERA-Interim

reanalysis data (*52*). For data assimilation calculations, the a priori anthropogenic emissions of NOx, CO, and SO_2 were obtained from the HTAP version 2 for 2010 (*53*), which were produced using the Regional Emission Inventory in Asia (REAS) for China. Emissions from biomass burning were based on the monthly Global Fire Emissions Database (GFED) version 4 (*54*) for NOx and CO. Emissions from soils were based on monthly means of the Global Emissions Inventory Activity (GEIA) (*55*) emissions for NOx. For other compounds, including VOCs, emissions were taken from the HTAP version 2 and GFED version 4 emissions.

Ozone production efficiency (OPE) estimates The COVID-19 ozone response and OPE were estimated from model simulations using the BAU and 2020 emissions. To estimate the TOB anomaly related to COVID-19, we conducted a model simulation from February 1, 2020 through July 31, 2020, which provides the accumulated influences of NOx emissions changes during the course of the COVID pandemic. To evaluate the relative importance of NOx emission reductions for each region, additional sensitivity calculations were conducted by replacing the BAU emissions with the 2020 emissions for each region (Fig. S1) separately. For estimating OPE (in TgO_3/TgN), model simulations were conducted from the beginning to the end of each month for February to June, 2020, using the same initial conditions, and the simulated tropospheric ozone burden averaged over the last 5 days of each month was compared between the simulations using the BAU and 2020 emissions. This method provides monthly changes in the ozone response to reduced NOx emissions for each region separately.

Statistical Analysis The multi-year standard deviation of the BAU emissions was used as an estimate of the uncertainty of the COVID NOx emission anomaly. For OPE, the standard deviation of estimated TOB during the analysis period was used to provide an uncertainty estimate. The validation of the model results against assimilated and independent observations is given in the Supplementary Materials (S1-S4).

References

1. M. Chinazzi, J. T. Davis, M. Ajelli, C. Gioannini, M. Litvinova, S. Merler, A. Pastore y Piontti, K. Mu, L. Rossi, K. Sun, C. Viboud, X. Xiong, H. Yu, M. E. Halloran, I. M. Longini, A. Vespignani, The effect of travel restrictions on the spread of the 2019 novel coronavirus (covid-19) outbreak. *Science* **368**, 395–400 (2020).

2. R. Cash, V. Patel, Has COVID-19 subverted global health? *The Lancet* **395**, 1687–1688 (2020).

3. C. Le Quéré, R. B. Jackson, M. W. Jones, A. J. P. Smith, S. Abernethy, R. M. Andrew, A. J. De-Gol, D. R. Willis, Y. Shan, J. G. Canadell, P. Friedlingstein, F. Creutzig, G. P. Peters, Temporary reduction in daily global CO2 emissions during the COVID-19 forced confinement. *Nature Climate Change* **10**, 647–653 (2020).

4. P. M. Forster, H. I. Forster, M. J. Evans, M. J. Gidden, C. D. Jones, C. A. Keller, R. D. Lamboll, C. L. Quéré, J. Rogelj, D. Rosen, C.-F. Schleussner, T. B. Richardson, C. J. Smith, S. T. Turnock, Publisher Correction: Current and future global climate impacts resulting from COVID-19. *Nature Climate Change* **10**, 971 (2020).

5. Z. Liu, P. Ciais, Z. Deng, R. Lei, S. J. Davis, S. Feng, B. Zheng, D. Cui, X. Dou, B. Zhu, R. Guo, P. Ke, T. Sun, C. Lu, P. He, Y. Wang, X. Yue, Y. Wang, Y. Lei, H. Zhou, Z. Cai, Y. Wu, R. Guo, T. Han, J. Xue, O. Boucher, E. Boucher, F. Chevallier, K. Tanaka, Y. Wei, H. Zhong, C. Kang, N. Zhang, B. Chen, F. Xi, M. Liu, F.-M. Bréon, Y. Lu, Q. Zhang, D. Guan, P. Gong, D. M. Kammen, K. He, H. J. Schellnhuber, Near-real-time monitoring of global CO2 emissions reveals the effects of the COVID-19 pandemic. *Nature Communications* **11**, 5172 (2020).

6. T. Le, Y. Wang, L. Liu, J. Yang, Y. L. Yung, G. Li, J. H. Seinfeld, Unexpected air pollution with marked emission reductions during the covid-19 outbreak in china. *Science* **369**, 702–706 (2020).

7. F. Liu, A. Page, S. A. Strode, Y. Yoshida, S. Choi, B. Zheng, L. N. Lamsal, C. Li, N. A. Krotkov, H. Eskes, R. van der A, P. Veefkind, P. F. Levelt, O. P. Hauser, J. Joiner, Abrupt decline in tropospheric nitrogen dioxide over china after the outbreak of covid-19. *Science Advances* **6** (2020).

8. G. He, Y. Pan, T. Tanaka, The short-term impacts of COVID-19 lockdown on urban air pollution in China. *Nature Sustainability* (2020).

9. K. P. Vadrevu, A. Eaturu, S. Biswas, K. Lasko, S. Sahu, J. K. Garg, C. Justice, Spatial and temporal variations of air pollution over 41 cities of India during the COVID-19 lockdown period. *Scientific Reports* **10**, 16574 (2020).

10. X. Shi, G. P. Brasseur, The response in air quality to the reduction of chinese economic activities during the covid-19 outbreak. *Geophysical Research Letters* **47**, e2020GL088070 (2020).

11. Z. S. Venter, K. Aunan, S. Chowdhury, J. Lelieveld, Covid-19 lockdowns cause global air pollution declines. *Proceedings of the National Academy of Sciences* **117**, 18984–18990 (2020).

12. M. Bauwens, S. Compernolle, T. Stavrakou, J.-F. Müller, J. van Gent, H. Eskes, P. F. Levelt, R. van der A, J. P. Veefkind, J. Vlietinck, H. Yu, C. Zehner, Impact of coronavirus outbreak on no2 pollution assessed using tropomi and omi observations. *Geophysical Research Letters* **47**, e2020GL087978 (2020).

13. J. H. Kroll, C. L. Heald, C. D. Cappa, D. K. Farmer, J. L. Fry, J. G. Murphy, A. L. Steiner, The complex chemical effects of COVID-19 shutdowns on air quality. *Nature Chemistry* **12**, 777–779 (2020).

14. N. S. Diffenbaugh, C. B. Field, E. A. Appel, I. L. Azevedo, D. D. Baldocchi, M. Burke, J. A. Burney, P. Ciais, S. J. Davis, A. M. Fiore, S. M. Fletcher, T. W. Hertel, D. E. Horton, S. M. Hsiang, R. B. Jackson, X. Jin, M. Levi, D. B. Lobell, G. A. McKinley, F. C. Moore, A. Montgomery, K. C. Nadeau, D. E. Pataki, J. T. Randerson, M. Reichstein, J. L. Schnell, S. I. Seneviratne, D. Singh, A. L. Steiner, G. Wong-Parodi, The COVID-19 lockdowns: a window into the Earth System. *Nature Reviews Earth & Environment* **1**, 470–481 (2020).

15. H. E. Institute, State of global air 2019 (2019).

16. K. Bowman, D. K. Henze, Attribution of direct ozone radiative forcing to spatially resolved emissions. *Geophysical Research Letters* **39** (2012).

17. G. Myhre, D. Shindell, F.-M. Bréon, W. Collins, J. Fuglestvedt, J. Huang, D. Koch, J.-F. Lamarque, D. Lee, B. Mendoza, T. Nakajima, A. Robock, G. Stephens, T. Takemura, H. Zhang, *Climate Change 2013: The Physical Science Basis. Contribution of Working Group I to the Fifth Assessment Report of the Intergovernmental Panel on Climate Change* (Cambridge University Press, 2014), chap. Anthropogenic and Natural Radiative Forcing, pp. 659–740.

18. A. Gaudel, R. Cooper, G. Ancellet, B. Barret, A. Boynard, J. Burrows, C. Clerbaux, P.-F. Coheur, J. Cuesta, E. Cuevas, *et al.*, Tropospheric ozone assessment report: Present-day distribution and trends of tropospheric ozone relevant to climate and global atmospheric chemistry model evaluation. *Elementa: Science of the Anthropocene* **6**, art–39 (2018).

19. K. Li, D. J. Jacob, H. Liao, J. Zhu, V. Shah, L. Shen, K. H. Bates, Q. Zhang, S. Zhai, A two-pollutant strategy for improving ozone and particulate air quality in china. *Nature Geoscience* **12**, 906–910 (2019).

20. K. Miyazaki, K. Bowman, T. Sekiya, H. Eskes, F. Boersma, H. Worden, N. Livesey, V. H. Payne, K. Sudo, Y. Kanaya, *et al.*, Updated tropospheric chemistry reanalysis and emission estimates, tcr-2, for 2005–2018. *Earth System Science Data* **12**, 2223–2259 (2020).

21. K. Miyazaki, K. Bowman, T. Sekiya, Z. Jiang, X. Chen, H. Eskes, M. Ru, Y. Zhang, D. Shindell, Air quality response in china linked to the 2019 novel coronavirus (covid-19) lockdown. *Geophysical Research Letters* **47**, e2020GL089252 (2020).

22. T. Hale, N. Angrist, E. Cameron-Blake, L. Hallas, B. Kira, S. Majumdar, A. Petherick, T. Phillips, H. Tatlow, S. Webster, Oxford covid-19 government response tracker. *Blavatnik School of Government* (2020).

23. C. L. Archer, G. Cervone, M. Golbazi, N. Al Fahel, C. Hultquist, Changes in air quality and human mobility in the USA during the COVID-19 pandemic. *Bulletin of Atmospheric Science and Technology* (2020).

24. D. Fu, K. W. Bowman, H. M. Worden, V. Natraj, J. R. Worden, S. Yu, P. Veefkind, I. Aben, J. Landgraf, L. Strow, Y. Han, High-resolution tropospheric carbon monoxide profiles retrieved from cris and tropomi. *Atmospheric Measurement Techniques* **9**, 2567–2579 (2016).

25. Y. Yang, Y. Wang, P. Zhou, D. Yao, D. Ji, J. Sun, Y. Wang, S. Zhao, W. Huang, S. Yang, D. Chen, W. Gao, Z. Liu, B. Hu, R. Zhang, L. Zeng, M. Ge, T. Petäjä, V.-M. Kerminen, M. Kulmala, Y. Wang, Atmospheric reactivity and oxidation capacity during summer at a suburban site between beijing and tianjin. *Atmospheric Chemistry and Physics* **20**, 8181–8200 (2020).

26. Y. Zhang, J. West, L. K. Emmons, K. Sudo, T. Sekiya, J. Flemming, j. E. Jonson, M. T. Lund, Contributions of world regions to the global tropospheric ozone burden change from 1980 to 2010. *Earth and Space Science Open Archive* p. 17 (2020).

27. P. J. Young, A. T. Archibald, K. W. Bowman, J.-F. Lamarque, V. Naik, D. S. Stevenson, S. Tilmes, A. Voulgarakis, O. Wild, D. Bergmann, P. Cameron-Smith, I. Cionni, W. J. Collins, S. B. Dalsøren, R. M. Doherty, V. Eyring, G. Faluvegi, L. W. Horowitz, B. Josse, Y. H. Lee, I. A. MacKenzie, T. Nagashima, D. A. Plummer, M. Righi, S. T. Rumbold, R. B. Skeie, D. T. Shindell, S. A. Strode, K. Sudo, S. Szopa, G. Zeng, Pre-industrial to end 21st century projections of tropospheric ozone from the atmospheric chemistry and climate model intercomparison project (accmip). *Atmospheric Chemistry and Physics* **13**, 2063–2090 (2013).

28. A. Gaudel, *et al.*, Tropospheric ozone assessment report: Present-day distribution and trends of tropospheric ozone relevant to climate and global atmospheric chemistry model evaluation. *Elementa Science of the Anthropocene* **6**, 39 (2018).

29. L. Kuai, K. W. Bowman, K. Miyazaki, M. Deushi, L. Revell, E. Rozanov, F. Paulot, S. Strode, A. Conley, J.-F. Lamarque, P. Jöckel, D. A. Plummer, L. D. Oman, H. Worden, S. Kulawik, D. Paynter, A. Stenke, M. Kunze, Attribution of chemistry-climate model initiative (ccmi) ozone radiative flux bias from satellites. *Atmospheric Chemistry and Physics* **20**, 281–301 (2020).

30. K. Miyazaki, K. W. Bowman, K. Yumimoto, T. Walker, K. Sudo, Evaluation of a multi-model, multi-constituent assimilation framework for tropospheric chemical reanalysis. *Atmospheric Chemistry and Physics* **20**, 931–967 (2020).

31. S. Watanabe, T. Hajima, K. Sudo, T. Nagashima, T. Takemura, H. Okajima, T. Nozawa, H. Kawase, M. Abe, T. Yokohata, *et al.*, Miroc-esm 2010: Model description and basic results of cmip5-20c3m experiments. *Geoscientific Model Development* **4**, 845 (2011).

32. D. S. Stevenson, F. J. Dentener, M. G. Schultz, K. Ellingsen, T. P. C. van Noije, O. Wild, G. Zeng, M. Amann, C. S. Atherton, N. Bell, D. J. Bergmann, I. Bey, T. Butler, J. Cofala, W. J. Collins, R. G. Derwent, R. M. Doherty, J. Drevet, H. J. Eskes, A. M. Fiore, M. Gauss, D. A. Hauglustaine, L. W. Horowitz, I. S. A. Isaksen, M. C. Krol, J.-F. Lamarque, M. G. Lawrence, V. Montanaro, J.-F. Müller, G. Pitari, M. J. Prather, J. A. Pyle, S. Rast, J. M. Rodriguez, M. G. Sanderson, N. H. Savage, D. T. Shindell, S. E. Strahan, K. Sudo, S. Szopa, Multimodel ensemble simulations of present-day and near-future tropospheric ozone. *Journal of Geophysical Research: Atmospheres* **111** (2006).

33. D. S. Stevenson, P. J. Young, V. Naik, J.-F. Lamarque, D. T. Shindell, A. Voulgarakis, R. B. Skeie, S. B. Dalsoren, G. Myhre, T. K. Berntsen, G. A. Folberth, S. T. Rumbold, W. J. Collins, I. A. MacKenzie, R. M. Doherty, G. Zeng, T. P. C. van Noije, A. Strunk, D. Bergmann, P. Cameron-Smith, D. A. Plummer, S. A. Strode, L. Horowitz, Y. H. Lee, S. Szopa, K. Sudo, T. Nagashima, B. Josse, I. Cionni, M. Righi, V. Eyring, A. Conley, K. W. Bowman, O. Wild, A. Archibald, Tropospheric ozone changes, radiative forcing and attribution to emissions in the atmospheric chemistry and climate model intercomparison project (accmip). *Atmospheric Chemistry and Physics* **13**, 3063–3085 (2013).

34. Z. Q. Hakim, S. Archer-Nicholls, G. Beig, G. A. Folberth, K. Sudo, N. L. Abraham, S. Ghude, D. K. Henze, A. T. Archibald, Evaluation of tropospheric ozone and ozone precursors in simulations from the htapii and ccmi model intercomparisons – a focus on the indian subcontinent. *Atmospheric Chemistry and Physics* **19**, 6437–6458 (2019).

35. L. C. Valin, A. R. Russell, R. C. Hudman, R. C. Cohen, Effects of model resolution on the interpretation of satellite no_2 observations. *Atmospheric Chemistry and Physics* **11**, 11647–11655 (2011).

36. J. Xu, X. Ge, X. Zhang, W. Zhao, R. Zhang, Y. Zhang, Covid-19 impact on the concentration and composition of submicron particulate matter in a typical city of northwest china. *Geophysical Research Letters* **47**, e2020GL089035 (2020).

37. K. Li, D. J. Jacob, H. Liao, L. Shen, Q. Zhang, K. H. Bates, Anthropogenic drivers of 2013–2017 trends in summer surface ozone in china. *Proceedings of the National Academy of Sciences* **116**, 422–427 (2019).

38. E. M. Fujita, D. E. Campbell, W. R. Stockwell, D. R. Lawson, Past and future ozone trends in california's south coast air basin: Reconciliation of ambient measurements with past and projected emission inventories. *Journal of the Air & Waste Management Association* **63**, 54-69 (2013).

39. D. D. Parrish, L. M. Young, M. H. Newman, K. C. Aikin, T. B. Ryerson, Ozone design values in southern california's air basins: Temporal evolution and u.s. background contribution. *Journal of Geophysical Research: Atmospheres* **122**, 11,166-11,182 (2017).

40. K. F. Boersma, H. J. Eskes, A. Richter, I. D. Smedt, A. Lorente, S. Beirle, J. H. Van Geffen, M. Zara, E. Peters, M. V. Roozendael, *et al.*, Improving algorithms and uncertainty estimates for satellite no 2 retrievals: results from the quality assurance for the essential climate variables (qa4ecv) project. *Atmospheric Measurement Techniques* **11**, 6651–6678 (2018).

41. J. v. Geffen, K. F. Boersma, H. Eskes, M. Sneep, M. t. Linden, M. Zara, J. P. Veefkind, S5p tropomi no 2 slant column retrieval: method, stability, uncertainties and comparisons with omi. *Atmospheric Measurement Techniques* **13**, 1315–1335 (2020).

42. K. Miyazaki, H. Eskes, K. Sudo, Global nox emission estimates derived from an assimilation of omi tropospheric no2 columns. *Atmospheric Chemistry and Physics* **12**, 2263 (2012).

43. N. A. Krotkov, C. A. McLinden, C. Li, L. N. Lamsal, E. A. Celarier, S. V. Marchenko, W. H. Swartz, E. J. Bucsela, J. Joiner, B. N. Duncan, *et al.*, Aura omi observations of regional so 2 and no 2 pollution changes from 2005 to 2015. *Atmospheric Chemistry and Physics* **16**, 4605 (2016).

44. M. N. Deeter, D. P. Edwards, G. L. Francis, J. C. Gille, S. Martínez-Alonso, H. M. Worden, C. Sweeney, A climate-scale satellite record for carbon monoxide: the mopitt version 7 product. *Atmospheric Measurement Techniques* **10**, 2533–2555 (2017).

45. N. Livesey, W. Read, P. Wagner, L. Froidevaux, A. Lambert, G. Manney, L. Millán Valle, H. Pumphrey, M. Santee, M. Schwartz, *et al.*, Version 4.2 x level 2 data quality and description document, jet propul, *Tech. rep.*, Lab., Tech. Rep. JPL D-33509 Rev. D, Pasadena, CA, USA. (2018).

46. K. Miyazaki, H. Eskes, K. Sudo, A tropospheric chemistry reanalysis for the years 2005–2012 based on an assimilation of omi, mls, tes, and mopitt satellite data. *Atmos. Chem. Phys* **15**, 8315–8348 (2015).

47. K. Miyazaki, H. Eskes, K. Sudo, K. F. Boersma, K. Bowman, Y. Kanaya, Decadal changes in global surface no x emissions from multi-constituent satellite data assimilation. *Atmospheric Chemistry & Physics* **17** (2017).

48. K. Miyazaki, T. Sekiya, D. Fu, K. Bowman, S. Kulawik, K. Sudo, T. Walker, Y. Kanaya, M. Takigawa, K. Ogochi, *et al.*, Balance of emission and dynamical controls on ozone during the korea-united states air quality campaign from multiconstituent satellite data assimilation. *Journal of Geophysical Research: Atmospheres* **124**, 387–413 (2019).

49. Z. Jiang, B. C. McDonald, H. Worden, J. R. Worden, K. Miyazaki, Z. Qu, D. K. Henze, D. B. Jones, A. F. Arellano, E. V. Fischer, *et al.*, Unexpected slowdown of us pollutant emission reduction in the past decade. *Proceedings of the National Academy of Sciences* **115**, 5099–5104 (2018).

50. L. Giglio, C. Justice, L. Boschetti, D. Roy, Mcd64a1 modis. *Terra+ Aqua Burned Area Monthly L3 Global 500m SIN Grid V006 MCD64A1 (https://doi. org/10.5067/MODIS/MCD64A1. 006)* (2015).

51. T. Sekiya, K. Miyazaki, K. Ogochi, K. Sudo, M. Takigawa, Global high-resolution simulations of tropospheric nitrogen dioxide using chaser v4. 0. *Geoscientific Model Development* **11**, 959 (2018).

52. D. P. Dee, S. M. Uppala, A. Simmons, P. Berrisford, P. Poli, S. Kobayashi, U. Andrae, M. Balmaseda, G. Balsamo, d. P. Bauer, *et al.*, The era-interim reanalysis: Configuration and performance of the data assimilation system. *Quarterly Journal of the royal meteorological society* **137**, 553–597 (2011).

53. G. Janssens-Maenhout, M. Crippa, D. Guizzardi, F. Dentener, M. Muntean, G. Pouliot, T. Keating, Q. Zhang, J. Kurokawa, R. Wankmüller, *et al.*, Htap_v2. 2: a mosaic of regional and global emission grid maps for 2008 and 2010 to study hemispheric transport of air pollution. *Atmospheric Chemistry and Physics* **15**, 11411–11432 (2015).

54. J. Randerson, G. Van der Werf, L. Giglio, G. Collatz, P. Kasibhatla, Global fire emissions database, version 4.1 (gfedv4). *ORNL DAAC* (2015).

55. T. Graedel, T. Bates, A. Bouwman, D. Cunnold, J. Dignon, I. Fung, D. Jacob, B. Lamb, J. Logan, G. Marland, *et al.*, A compilation of inventories of emissions to the atmosphere. *Global Biogeochemical Cycles* **7**, 1–26 (1993).

Acknowledgments

General: We acknowledge the use of data products from the NASA Aura and EOS Terra and Aqua satellite missions. We also acknowledge the free use of the tropospheric NO_2 column data from the SCIAMACHY, GOME-2, and OMI sensors from http://www.qa4ecv.eu and from TROPOMI. The OpenAQ surface ozone data was obtained through EPA and the World Air Quality Index Project. The TROPOMI NO_2 algorithm and data processors have been developed by KNMI under the NSO TROPOMI Science Contract, in cooperation with ESA. Sentinel-5 Precursor is an ESA mission on behalf of the European Commission (EC). The Earth Simulator was used for model simulations with support of the Japan Agency for Marine-Earth Science and Technology. **Funding**: K.M. and K.B. acknowledge the support of the NASA Atmospheric Composition: Aura Science Team Program (19-AURAST19-0044) and the TROPESS project. Part of this work was conducted at the Jet Propulsion Laboratory, California Institute of Technology, under contract with the National Aeronautics and Space Administration (NASA). **Author contributions**: K.M., K.B., J.N. designed the research; all the authors performed research and wrote and edited the paper. **Competing interests**: There are no conflicts of interest to declare. **Data and materials availability**: All data needed to evaluate the conclusions in the paper are present in the paper and/or the Supplementary Materials, as well as references cited therein. Additional data related to this paper may be requested from the authors.

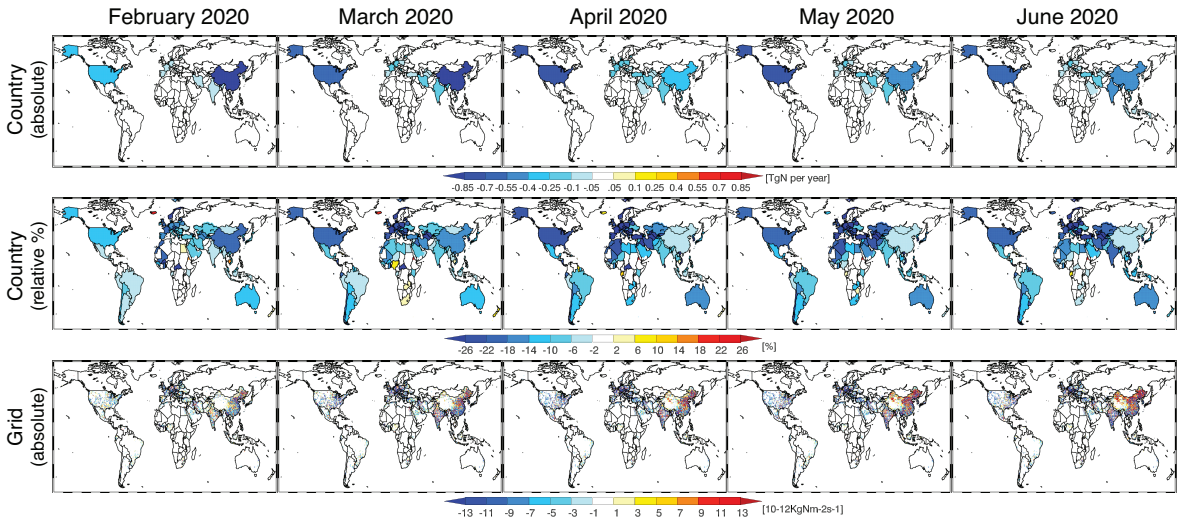

Fig. 1. Spatial distributions of the monthly mean NOx emission reductions due to the COVID-19 lockdowns. The COVID NOx emission anomaly in February-June 2020 was estimated from differences between the 2020 and BAU emissions. Results are shown for the absolute changes in country total emissions (in TgN per year, upper panels), relative changes in country total emissions (in %, center panels), and absolute changes in grid-scale emissions (in $10^{-12} kgNm^{-2}s^{-1}$, lower panels),

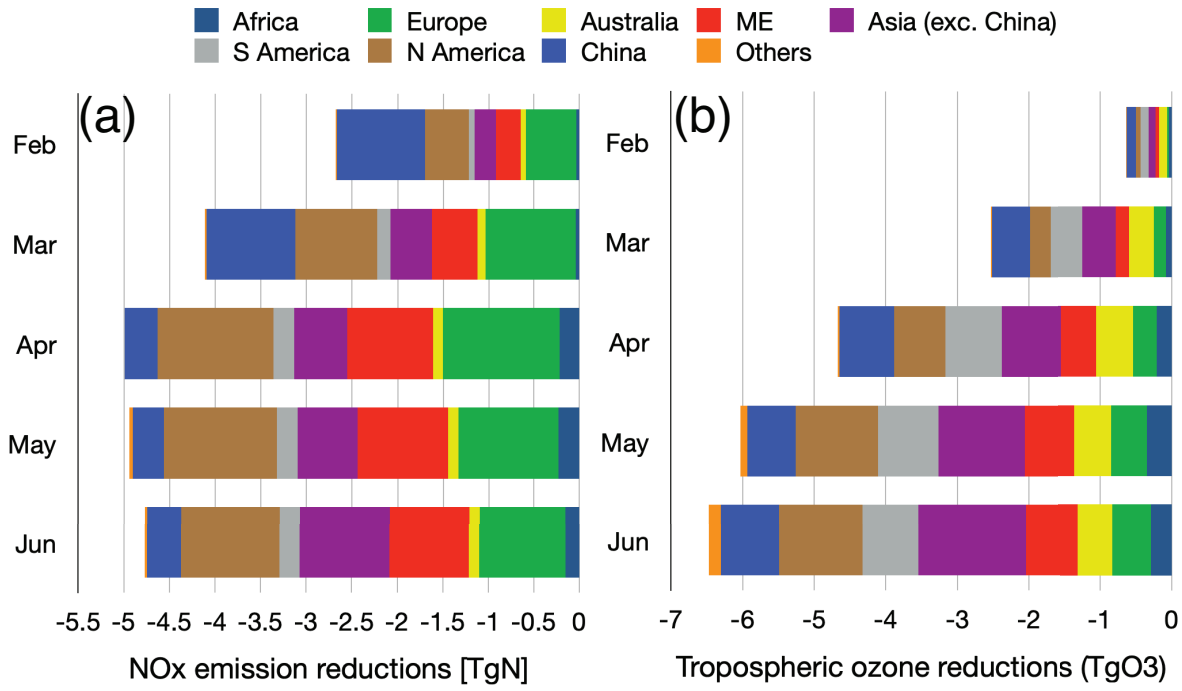

Fig. 2. Reductions in anthropogenic NOx emissions and tropospheric ozone burden. Monthly mean global and regional total changes in **(a)** NOx emissions (in TgN per year) due to the COVID-19 lockdowns and in **(b)** tropospheric ozone burden (in TgO_3) are shown for Africa, Europe, Australia, the Middle East, Asia (except for China), South America, North America, China, and other regions.

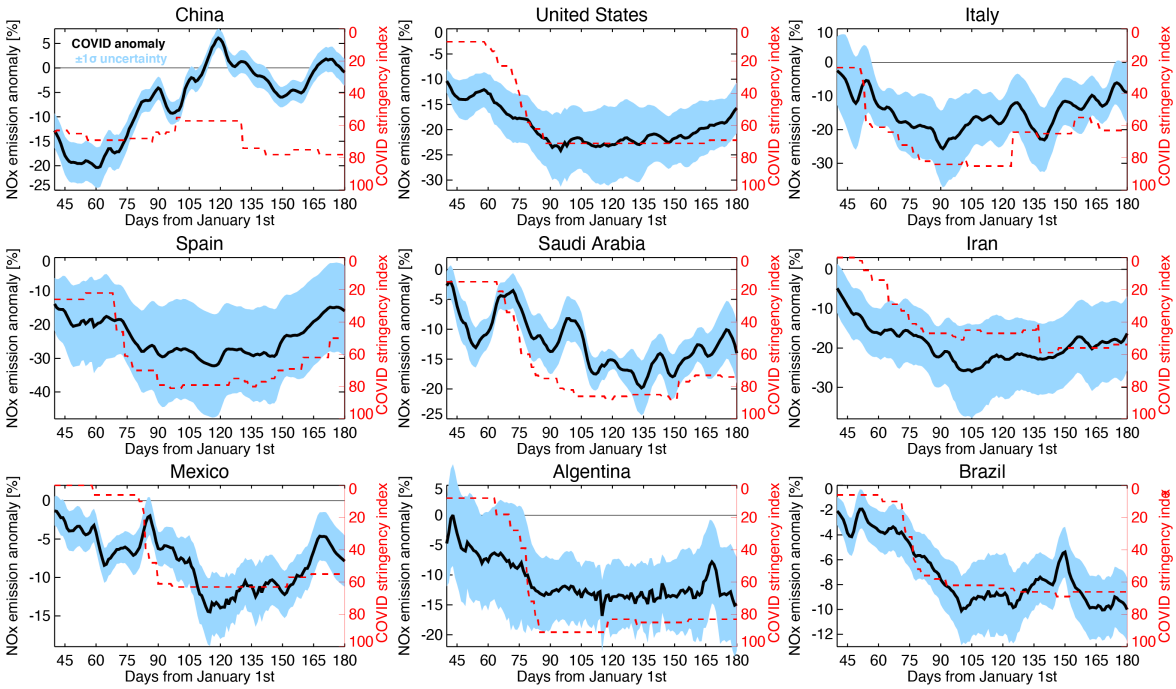

Fig. 3. Time series of relative changes in country-total NOx emissions (in %, black line) due to the COVID-19 lockdowns. The COVID-19 government response stringency index is shown by the dashed red line. The x-axis represents days from January 1, 2020. The shaded area represents the 1-sigma uncertainty as measured from the standard deviation of the BAU emissions.

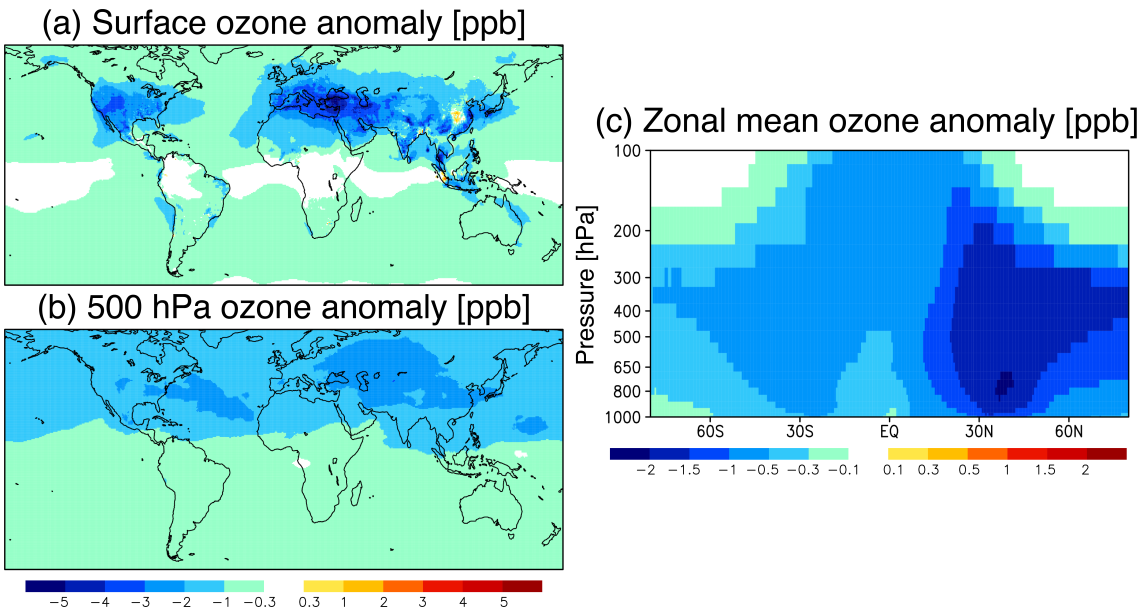

Fig. 4. Monthly ozone changes due to the COVID NOx emission reductions in May 2020. Spatial distribution of the ozone anomaly (in ppb) at **(a)** the surface, **(b)** 500 hPa, and **(c)** zonal mean values in latitude-pressure coordinates.

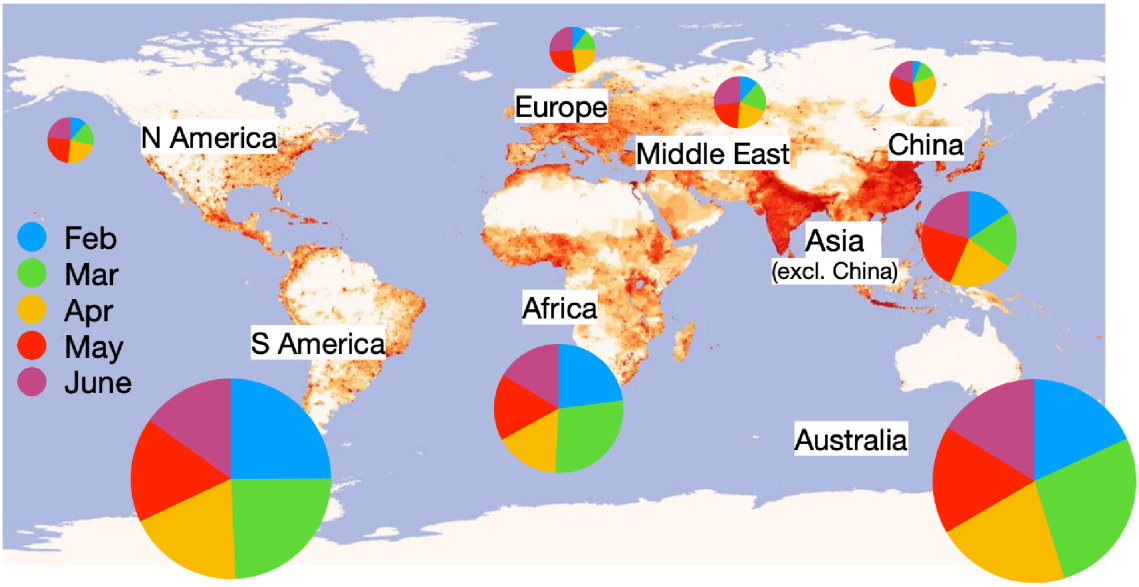

Fig. 5. Global map of the ozone production efficiency (OPE). OPE is estimated from the change in the global tropospheric ozone burden (TOB) corresponding to the COVID NOx emission anomaly for each region of the world. The diameter of each circle represents the averaged OPE value during February-July 2020, while each sector of the circle represents the relative OPE magnitude for each month. The background map shows population density.

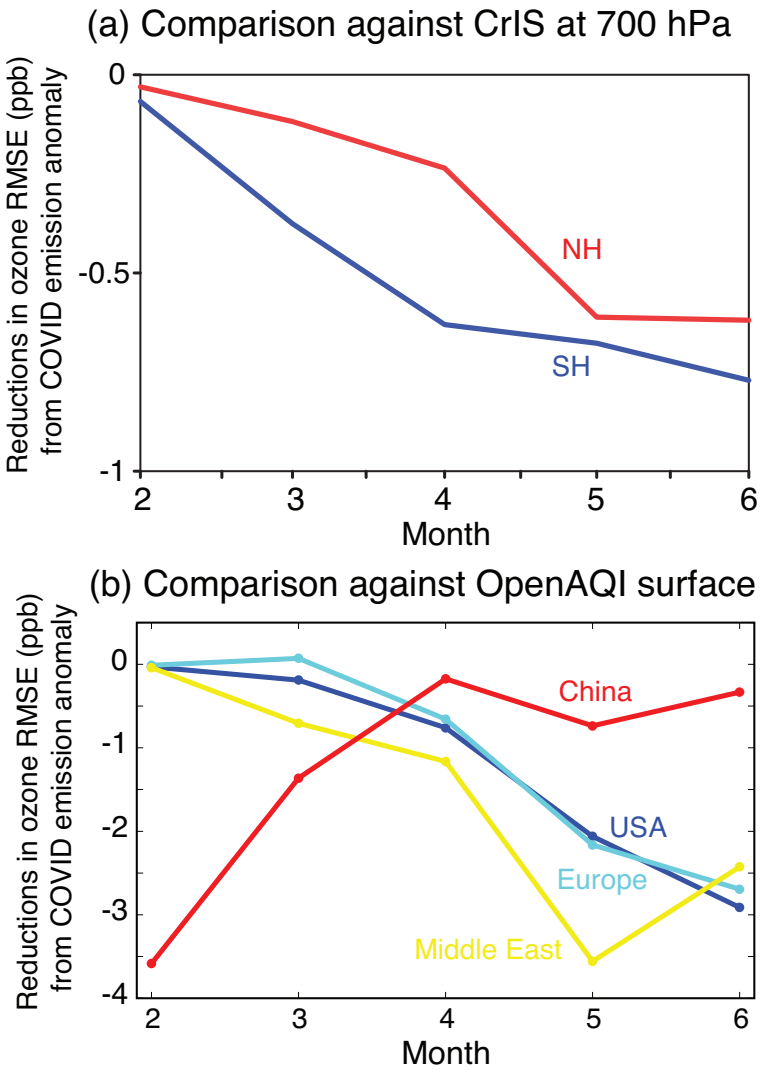

Fig. 6. Comparisons to ozone measurements from the CrIS satellite and surface networks. Time series of differences in monthly RMSEs (in ppb) of ozone against **(a)** the CrIS satellite retrievals at 700 hPa for the NH (20°N-90°N) and SH (90°S-20°S) and **(b)** the surface observations from the OpenAQ platform for Europe (light blue), the United States (blue), the Middle East (yellow), and China (red). The RMSE differences were estimated from two model simulations using the BAU and 2020 emissions, where the negative values show improved agreement against the observations using the 2020 emissions.

Table. 1. Monthly mean values of global and regional total surface NOx emission changes (in %) due to the COVID-19 restrictions. The 1-sigma uncertainties, estimated from the standard deviation of the multi-year BAU emissions, are also shown.

Region	Feb	Mar	Apr	May	Jun
Globe	-9.0±1.5	-12.7±1.5	-14.8±2.3	-15.0±1.8	-13.9±1.8
Africa	-1.8±3.7	-2.1±4.2	-9.9±4.4	-10.3±4.0	-6.7±4.1
Europe	-10.3±4.1	-16.5±4.6	-19.3±5.8	-18.7±5.6	-13.8±3.6
Australia	-10.2±4.0	-12.8±5.3	-14.6±5.7	-15.7±6.2	-15.9±7.4
Middle East	-8.3±4.8	-14.8±6.8	-24.1±9.7	-24.8±9.6	-21.7±10.6
Asia (excl. China)	-4.0±1.3	-7.4±1.6	-9.4±2.6	-10.6±2.1	-14.4±2.1
S America	-3.3±1.5	-7.0±1.8	-10.2±2.5	-10.2±2.4	-10.3±2.9
N America	-9.6±2.6	-16.1±4.3	-20.7±6.2	-20.1±5.5	-17.5±4.6
China	-18.3±3.8	-16.4±3.1	-6.2±2.2	-6.3±2.4	-6.9±2.5

Table. 2. Monthly values of the regional ozone production efficiency (OPE, in TgO_3/TgN). The OPE was estimated for the global tropospheric ozone burden (TOB), using the regional COVID-19 NOx emission anomalies. The 1-sigma uncertainties, estimated from the standard deviation (i.e., temporal changes) of the estimated TOB during the analysis period, are also shown.

Region	Feb	Mar	Apr	May	Jun
Africa	2.15±0.08	2.61±0.23	1.51±0.17	1.56±0.08	1.53±0.12
Europe	0.09±0.01	0.13±0.01	0.20±0.06	0.23±0.03	0.23±0.03
Australia	2.68±0.10	4.01±0.10	3.16±0.04	2.54±0.05	2.40±0.08
Middle East	0.25±0.01	0.40±0.05	0.45±0.05	0.47±0.05	0.57±0.05
Asia (excl. China)	1.11±0.04	1.35±0.03	1.54±0.15	1.65±0.07	1.44±0.04
S America	3.65±0.11	3.55±0.09	2.75±0.04	2.47±0.04	2.21±0.04
N America	0.23±0.01	0.33±0.04	0.45±0.08	0.50±0.06	0.45±0.06
China	0.08±0.00	0.17±0.01	0.37±0.05	0.44±0.04	0.25±0.02